



Parameter sensitivity analysis and cathode structure optimization of a non-aqueous Li–O₂ battery model

Kai Jiang^a, Xunliang Liu^{a,*}, Guofeng Lou^a, Zhi Wen^a, Lin Liu^b

^a School of Energy and Environmental Engineering, University of Science and Technology Beijing, Beijing, 100083, China

^b Department of Mechanical Engineering, The University of Kansas, Lawrence, KS, 66045, USA

HIGHLIGHTS

- A parameter sensitivity analysis is conducted on a non-aqueous Li–O₂ battery model.
- The cathode initial porosity is the most sensitive parameter to specific capacity.
- The hierarchical cathode can improve battery specific capacity by up to 10.38%.

ARTICLE INFO

Keywords:

Li–O₂ battery
Parameter sensitivity analysis
Hierarchical cathode
Simulation

ABSTRACT

Non-aqueous Li–O₂ batteries have gained more attention and are promising power sources for next-generation electric vehicles due to their high energy density. In the present study, a comprehensive one-dimensional model is developed to investigate the performance of non-aqueous Li–O₂ batteries. Two different models for insoluble discharge product growth are compared and the tunneling-effect model is in better agreement with the published experimental data. In order to evaluate the effects of various parameters on battery specific capacity in the model, the parameter sensitivity analysis is conducted under different current densities at a cutoff voltage of 2.4 V. The calculated average sensitivities are classified as three levels, including insensitive, sensitive, and very sensitive. The porosity of the cathode is found to be the most sensitive parameter to specific capacity. Based on this, a hierarchical porous cathode structure with gradient initial porosity distribution is proposed according to the distribution of cathode product and effective porosity. Our model shows that the hierarchical cathode structure can improve specific capacity by up to 10.38%.

1. Introduction

Among several different kinds of Li–Air battery (LAB) or Li–O₂ battery (LOB), non-aqueous LAB or LOB manifests a remarkably high specific capacity and excellent cyclability and has been gaining a lot of attention [1–3]. Existing studies mostly focus on the following: the mechanisms of charging and discharging processes [4,5], the properties of different electrolytes [6], the growth of metal lithium dendrites [7], and the structure of porous cathodes prepared through various methods [8–10,32]. With the enhanced understanding of the reaction mechanisms, an increasing number of research groups are conducting the simulation of non-aqueous LOB or LAB [18–25,49,50]. Modeling and simulation mostly focus on the microstructure of porous cathodes and macroscopic discharge processes of the battery rather than the electrolytes' properties and the complex electrochemical reactions during the

discharge process. Such discharge process can be different from the experimentation [11].

Experimental research on non-aqueous LAB is mainly divided into two categories, namely, discharging in the air and pure oxygen environment. The discharge process of non-aqueous LAB in the air environment is complicated due to the many different components of air, such as carbon dioxide and water vapor, that adds complexity to the electrochemical reactions [12]. However, the oxygen redox reaction, remains the dominate reaction of discharge in the open-air environment as it is in the pure oxygen environment. The chemical equations of the reaction are as follows [13]:

The half-reaction at the lithium anode is



The half-reaction at the porous cathode is

* Corresponding author.

E-mail address: liuxl@me.ustb.edu.cn (X. Liu).

<https://doi.org/10.1016/j.jpowsour.2020.227821>

Received 23 October 2019; Received in revised form 3 January 2020; Accepted 27 January 2020

Available online 5 February 2020

0378-7753/© 2020 Elsevier B.V. All rights reserved.

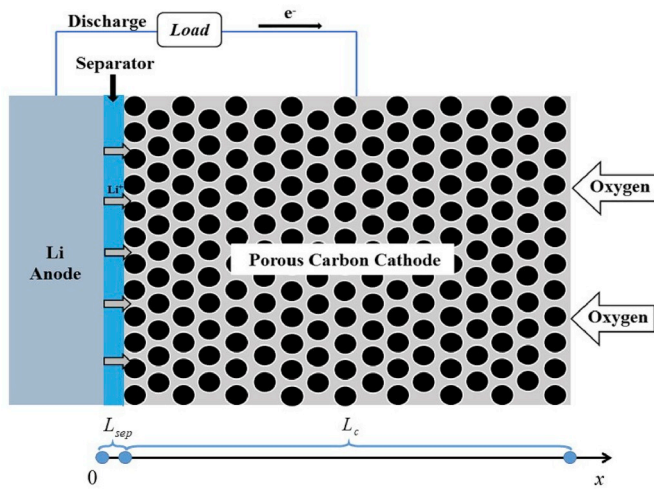


Fig. 1. Schematic of a non-aqueous LOB.

Table 1
Parameters used in the model.

Parameter	Symbol	Value	Unit	Reference
Thickness of porous cathode	L_c	8×10^{-4}	m	[30]
Thickness of separator	L_{sep}	2.5×10^{-5}	m	[31]
Porosity of cathode	ϵ_0	0.75	–	[31]
Porosity of separator	ϵ_{sep}	0.5	–	[31]
Specific interfacial area of cathode	a_0	3.67×10^7	$\text{m}^2 \text{m}^{-3}$	[31]
Li^+ diffusion coefficient	D_{Li}	2.11×10^{-9}	$\text{m}^2 \text{s}^{-1}$	[33]
Oxygen diffusion coefficient	D_{O_2}	1×10^{-9}	$\text{m}^2 \text{s}^{-1}$	[34]
Conductivity of positive electrode	σ_c	10	S m^{-1}	[29]
Conductivity of Li^+ in electrolyte	κ	0.5	S m^{-1}	[35]
Electrolyte concentration	$c_{Li,0}$	1 000	mol m^{-3}	[30]
Solubility factor of oxygen	S_{O_2}	0.38	–	[29]
External oxygen concentration in air at 1 atm	$c_{O_2,ext}$	9.46	mol m^{-3}	[29]
Initial oxygen concentration	$c_{O_2}^0$	3.5948	mol m^{-3}	Calculated
Solubility limit of Li_2O_2 dissolved in electrolyte	c_{max,Li_2O_2}	0.09	mol m^{-3}	[28]
Symmetry factor	β	0.5	–	[36]
Transference number of Li^+	t_+	0.2594	–	[37]
Equilibrium potential for oxygen reduction reaction	E_{eq}	2.96	V	[23]
Exchange current density for anode	i_0	1	A m^{-2}	Assumed
Reaction rate of anodic current	k_a	1.11×10^{-15}	m s^{-1}	Assumed
Reaction rate of cathodic current	k_c	3.40×10^{-20}	$\text{m}^7 \text{s}^{-1} \text{mol}^{-2}$	Assumed
Electrical resistivity across Li_2O_2 film formation	R_{film}	50	Ωm^2	[38]
Molecular weight of Li_2O_2	$M_{Li_2O_2}$	45.88×10^{-3}	kg mol^{-1}	–
Mass density of carbon	ρ_{carbon}	2 260	kg m^{-3}	[39]
Mass density of Lithium peroxide (Li_2O_2)	$\rho_{Li_2O_2}$	2 140	kg m^{-3}	[39]
Mass density of electrolyte solution (LiPF_6)	$\rho_{electrolyte}$	1 200	kg m^{-3}	[39]
Particle radius in the cathode	r_0	25×10^{-9}	m	[40]
Operating temperature	T	300	K	–

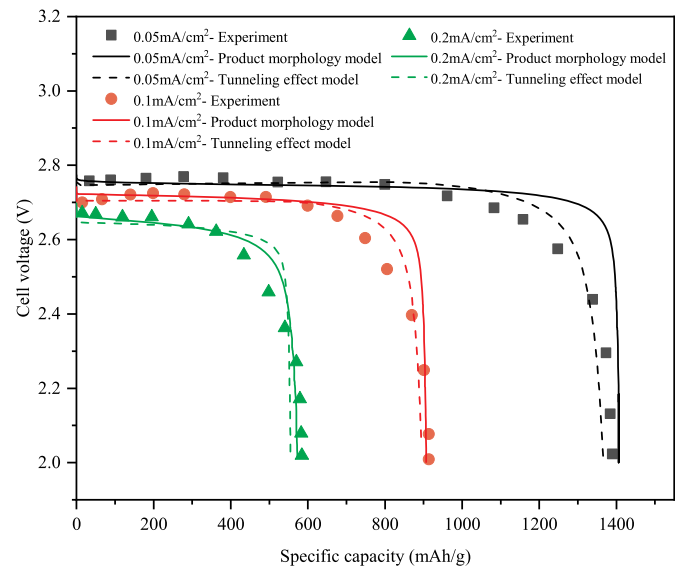


Fig. 2. Comparison of model prediction and experimental data [30] of voltage-capacity curve.



With the overall cell reaction being



The primary discharge product is lithium peroxide, which has poor solubility in organic electrolytes, leading to it depositing on the porous cathode [14]. The morphology of discharge products is dependent on operation conditions, such as current densities [42], specific structure of the porous cathode [43], and the organic electrolytes used [44,45]. The most common morphologies include film, hemisphere, toroid, and wrinkle [15,16]. The deposited lithium peroxide becomes an issue due to its low conductivity. As it builds up it will cause blockages in the porous structure, inhibiting the diffusion of oxygen and lithium ions. This leads to decreased utilization of active material, increased cell resistance and decreased cell capacity [17].

Many simulation studies on non-aqueous LOBs and LABs have been conducted under the framework of a one-dimensional (1D) model and resulted in acceptable accuracy [18–25]. Esfahanian et al. have developed a model considering that the oxygen crosses the separator to the lithium anode interface and reacts with the anode directly in LOB [24]. Gaya et al. have assumed that the macroporosity and mesoporosity domains in a compound cathode coexist by using a modified oxygen diffusion formula to calculate diffusion coefficient [25]. Based on the 1D model, researchers have analyzed the influence of individual key parameters on LAB specific capacity. Sahapatombut [23] established a LAB model for charge and discharge cycles, and studied discharge curves for different values of electrode porosity, electrode thickness and cathode reaction coefficient. In addition to the many simulation studies there are also experimental studies that have discussed the effect of cathode structure on the discharge process. The cathode structure includes different electrode types and porosity distribution [46–48]. Due to experimental limitations, many parameters cannot be studied by means of controlled variables, such as cathode material's conductivity, oxygen solubility, and carbon particle radius of the cathode. So performing a parameter sensitivity analysis is necessary to figure out to what extent that these parameters effects on battery performance, which could benefit battery design optimization.

In this study, we developed a comprehensive 1D electrochemical kinetic model for a non-aqueous LOB. In the model, two different methods, namely, the product morphology model and tunneling effect model, are implemented to evaluate the active surface area of the porous

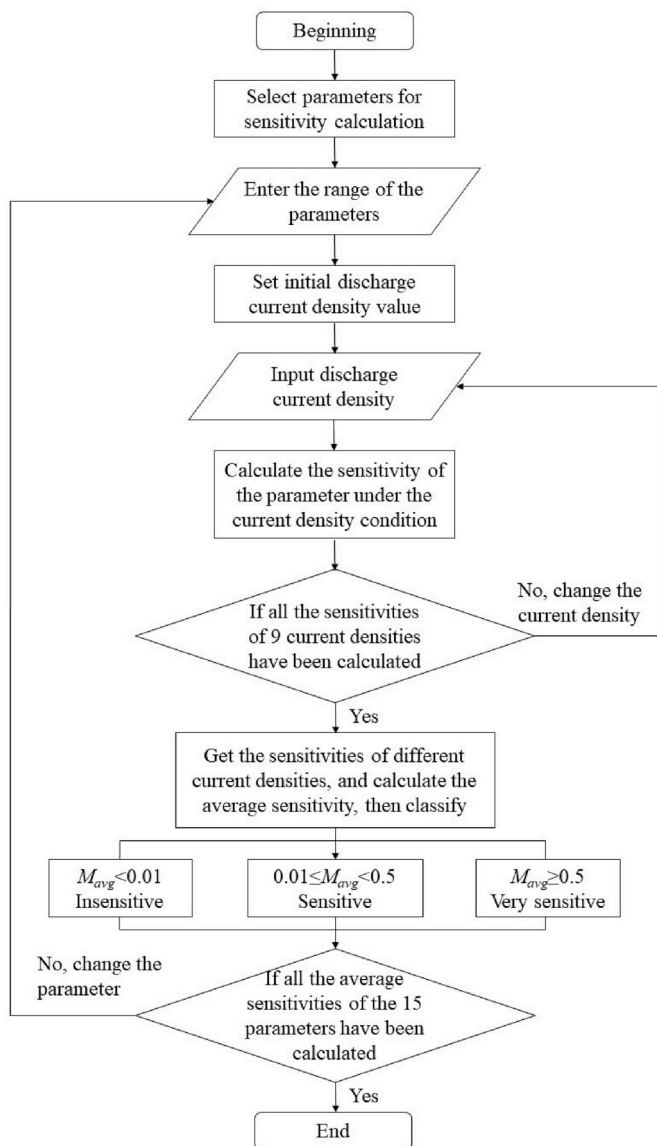


Fig. 3. Flow chart of parameter sensitivity analysis calculation.

cathode. Parameter sensitivity analysis is conducted based on the Li–O₂ battery model. The effects of 14 parameters on battery's specific capacity are analyzed with a cutoff voltage of 2.4 V as the specific capacity would hardly change later. Further, according to the parameter sensitivity analysis results, the parameter of cathode porosity is the most sensitive as it has the largest impact on the uneven discharge product distribution in the cathode. Hence, a hierarchical porous cathode with variable-porosity layers is proposed and simulated to optimize the cathode structure.

2. Model development

In the present study, Fig. 1 shows a 1D electrochemical kinetic model for a non-aqueous LOB, and the porous carbon cathode is composed of idealized small spherical particles, assuming that the cathode is a homogeneous porous medium, and the porosity is set to a certain value. The model incorporates Li⁺ and oxygen species transport with the conservation of charge. Two different insoluble discharge product growth models are used to take the change of air cathode porosity and the specific surface area into account. The first model, called the product morphology model, calculates the specific surface area according to the

Table 2
Range of the parameter sensitivity analysis.

Parameter	Symbol	Initial value x_0	Analysis range	Unit
Reaction rate of anodic current	k_a	1.11×10^{-15}	$1.11 \times 10^{-16} \sim 1.11 \times 10^{-14}$	m s^{-1}
Porosity of separator	ε_{sep}	0.5	0.25~0.75	m
Conductivity of cathode	σ_c	10	5~15	S m^{-1}
Thickness of separator	L_{sep}	2.5×10^{-5}	$1.3 \times 10^{-5} \sim 3.7 \times 10^{-5}$	m
Conductivity of Li ⁺ in electrolyte	κ	0.5	0.25~0.75	S m^{-1}
Initial Li ⁺ concentration	$c_{Li,0}$	1000	500~1500	mol m^{-3}
Li ⁺ diffusion coefficient	D_{Li}	2.11×10^{-9}	$1.06 \times 10^{-9} \sim 3.17 \times 10^{-9}$	$\text{m}^2 \text{s}^{-1}$
Reaction rate of cathodic current	k_c	3.4×10^{-20}	$3.4 \times 10^{-21} \sim 3.4 \times 10^{-19}$	S m^{-1}
Middle product film thickness	l_m	7	5~9	nm
Particle radius in the cathode	r_0	25×10^{-9}	$20 \times 10^{-9} \sim 30 \times 10^{-9}$	m
Oxygen diffusion coefficient	D_{O_2}	1×10^{-9}	$0.5 \times 10^{-9} \sim 1.5 \times 10^{-9}$	$\text{m}^2 \text{s}^{-1}$
Solubility factor of oxygen	S_{O_2}	0.38	0.19~0.54	-
Thickness of porous cathode	L_c	8×10^{-4}	$4 \times 10^{-4} \sim 14 \times 10^{-4}$	m
Porosity of cathode	ε_0	0.75	0.73~0.77	-

morphology shape of the solid peroxide Li₂O₂. The second model, called the tunneling-effect model, adopts a probability function to calculate the influence of electron tunneling effect on the active surface. As follows, 2.1 covers assumptions, 2.2 is the specifics of the battery model, 2.3 is applied boundary conditions.

2.1. Assumption

The assumptions used in the model are given as follows:

- (1) The main discharge product is Li₂O₂, which is only formed in the porous cathode where it accumulates on the active surface.
- (2) The porous cathode is completely filled with electrolyte, and the diffusion of Li⁺ is simulated by the concentrated solution theory.
- (3) Oxygen is soluble in the solution phase electrolyte, and the solution is initially saturated with it.
- (4) Convection is negligible inside the cell.
- (5) The thermal effect is not considered, that is, the battery is operated in an isothermal condition.

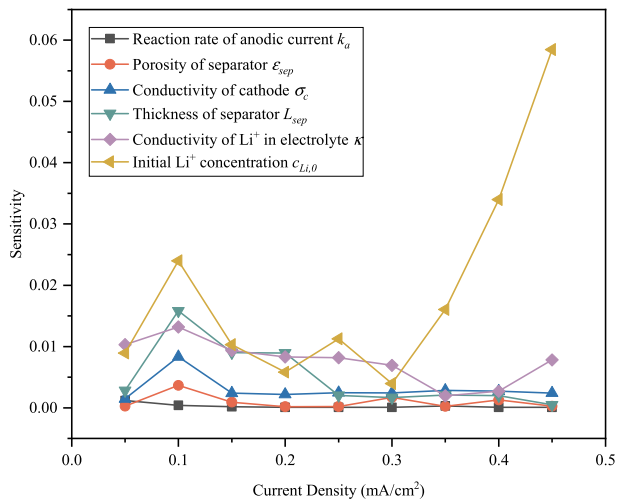
2.2. Battery model

2.2.1. Transport model of lithium ions

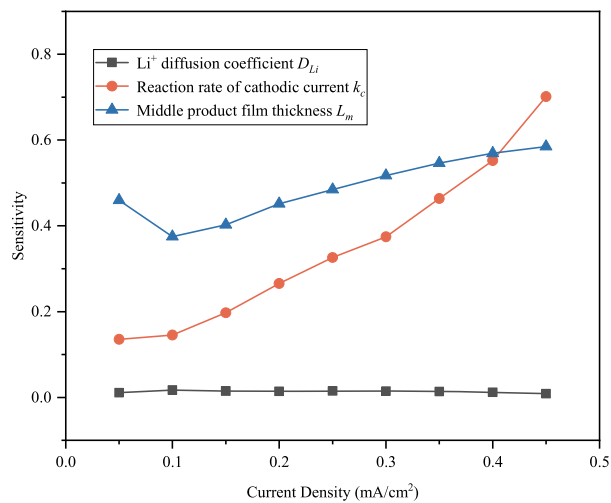
During discharge, lithium ions are transported through an organic electrolyte to the active site of the cathode. Without convection, the equation for transport of Li⁺ contains diffusion and migration and can be expressed as [23]

$$\frac{\partial c_{Li}}{\partial t} = -\nabla \cdot \left(-D_{Li,eff} \nabla c_{Li} + \frac{i t_+}{F} \right) + R_{Li}, \quad (4)$$

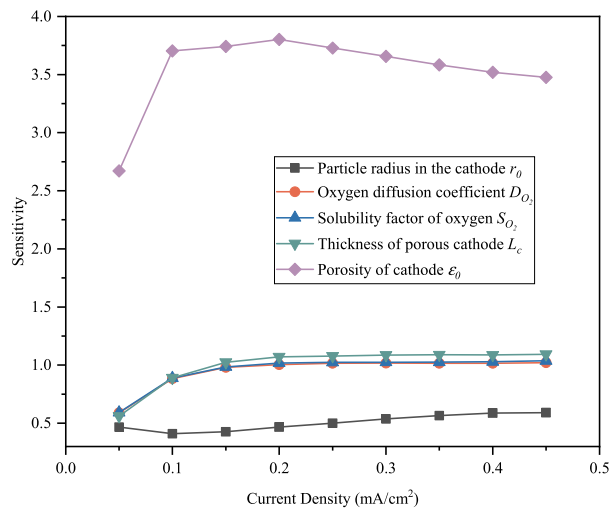
where ε is the porosity of the cathode. $D_{Li,eff}$ is the effective diffusion coefficient of Li⁺. t_+ is the transference number of Li⁺. F is Faraday's constant, which is equal to 96485 C mol⁻¹. i is the current density in the solution phase, and R_{Li} is the source item of Li⁺ due to the cathode reaction.



(a)



(b)



(c)

Fig. 4. Parameter sensitivity analysis results: (a) parameters not sensitive to the model, (b) parameters sensitive to the model, (c) parameters very sensitive to the model.

Table 3
Parameter sensitivity classification.

Number	Parameter	Symbol	Sensitivity M_{avg}	Catalogue
1	Reaction rate of anodic current	k_a	1.33×10^{-4}	Not sensitive
2	Porosity of separator	ϵ_{sep}	4.83×10^{-4}	Not sensitive
3	Conductivity of cathode	σ_c	1.51×10^{-3}	Not sensitive
4	Thickness of separator	L_{sep}	2.49×10^{-3}	Not sensitive
5	Conductivity of Li ⁺ in electrolyte	κ	3.82×10^{-3}	Not sensitive
6	Initial Li ⁺ concentration	$c_{Li,0}$	9.60×10^{-3}	Not sensitive
7	Li ⁺ diffusion coefficient	D_{Li}	1.34×10^{-2}	Sensitive
8	Reaction rate of cathodic current	k_c	3.51×10^{-1}	Sensitive
9	Middle product film thickness	l_m	4.88×10^{-1}	Sensitive
10	Particle radius in the cathode	r_0	5.06×10^{-1}	Very sensitive
11	Oxygen diffusion coefficient	D_{O_2}	9.49×10^{-1}	Very sensitive
12	Solubility factor of oxygen	S_{O_2}	9.58×10^{-1}	Very sensitive
13	Thickness of porous cathode	L_c	9.94×10^{-1}	Very sensitive
14	Porosity of cathode	ϵ_0	3.54	Very sensitive

2.2.2. Transport model of oxygen

Oxygen comes from the external air and dissolves in the electrolyte. The equation for oxygen transport also contains diffusion and migration, expressed as

$$\frac{\partial \epsilon c_{O_2}}{\partial t} = -\nabla \cdot (-D_{O_2,eff} \nabla c_{O_2}) + R_{O_2}, \quad (5)$$

where $D_{O_2,eff}$ is the effective diffusion coefficient of oxygen, and R_{O_2} is the source item of oxygen.

The transport equations above contain source items, which are concerned with the electrochemical reaction rate. The reaction rate can be given by Faraday's law.

$$R_i = -\frac{a s_i}{n F} j_c, \quad (6)$$

where a is the specific interfacial area of the cathode. s_i is the stoichiometric coefficient of the species i . n is the number of electrons transferred, and j_c is the local transfer current density between the cathode and the electrolyte interface.

2.2.3. Conservation of charge

The charge conservation between the solid and the solution phase can be expressed as

$$\nabla \cdot i_s + \nabla \cdot i_l = 0, \quad (7)$$

$$\nabla \cdot i_l = a j. \quad (8)$$

where i_l and i_s are the current density in the electrolyte solution and the solid phase, respectively. The current density in the solution phase can be given by Ref. [23].

$$i_l = -k_{eff} \nabla \phi_l - \frac{2RTk_{eff}}{F} (t_+ - 1) \left(1 + \frac{\partial \ln f}{\partial c_{Li}} \right) \nabla \ln c_{Li}. \quad (9)$$

The current density in the solid phase can be given by

$$i_s = -\sigma_{eff} \nabla \phi_s, \quad (10)$$

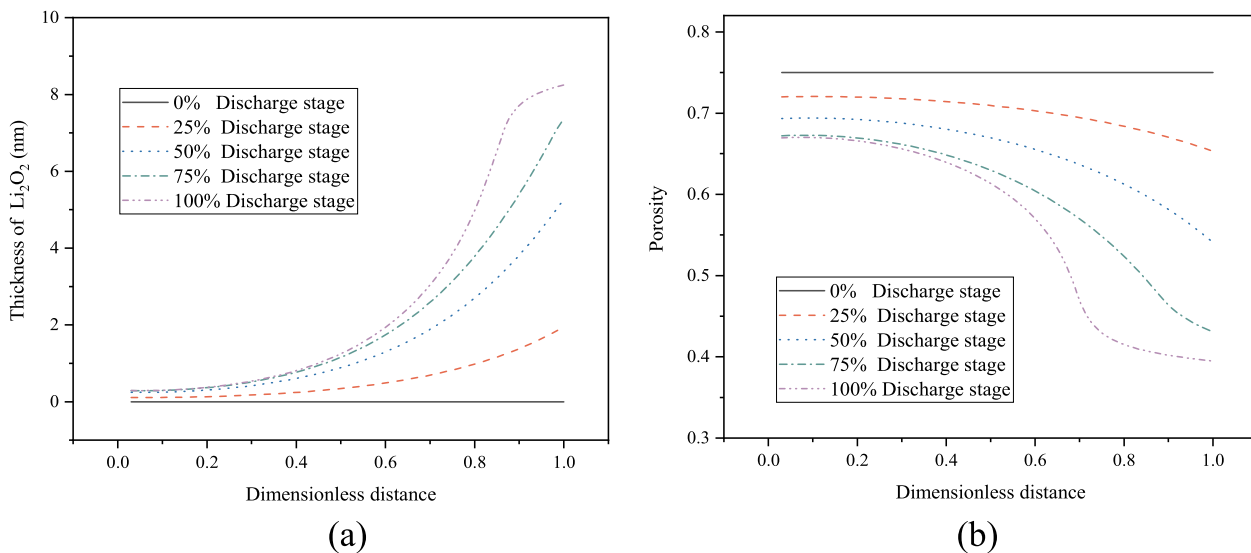


Fig. 5. Product film thickness distribution (a) and porosity distribution (b) at discharge current density of 0.2 mA cm^{-2} .

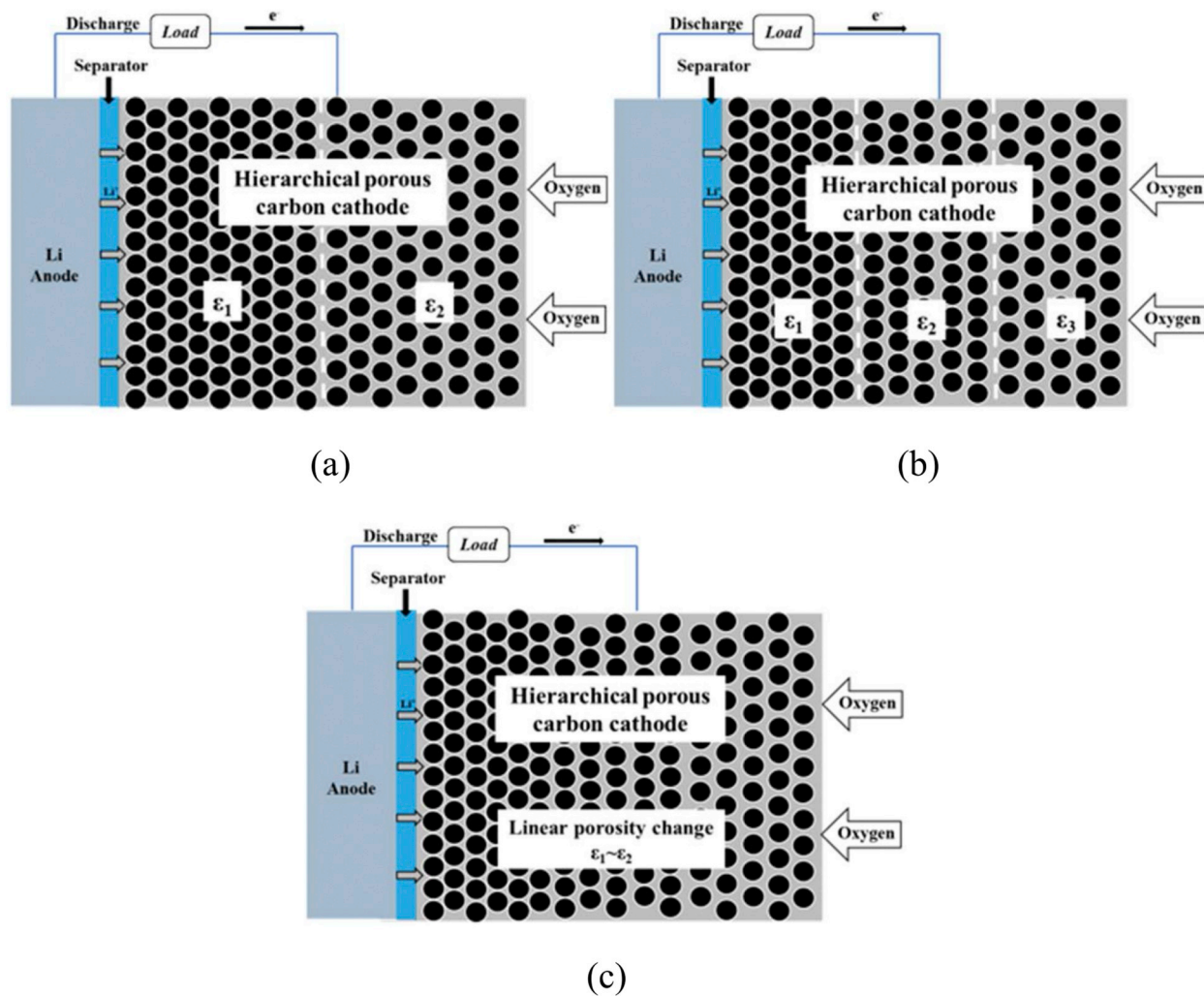


Fig. 6. Schematic diagrams of LOB with different porous cathode structures: (a) two-layer, (b) three-layer, and (c) gradient porosity cathodes.

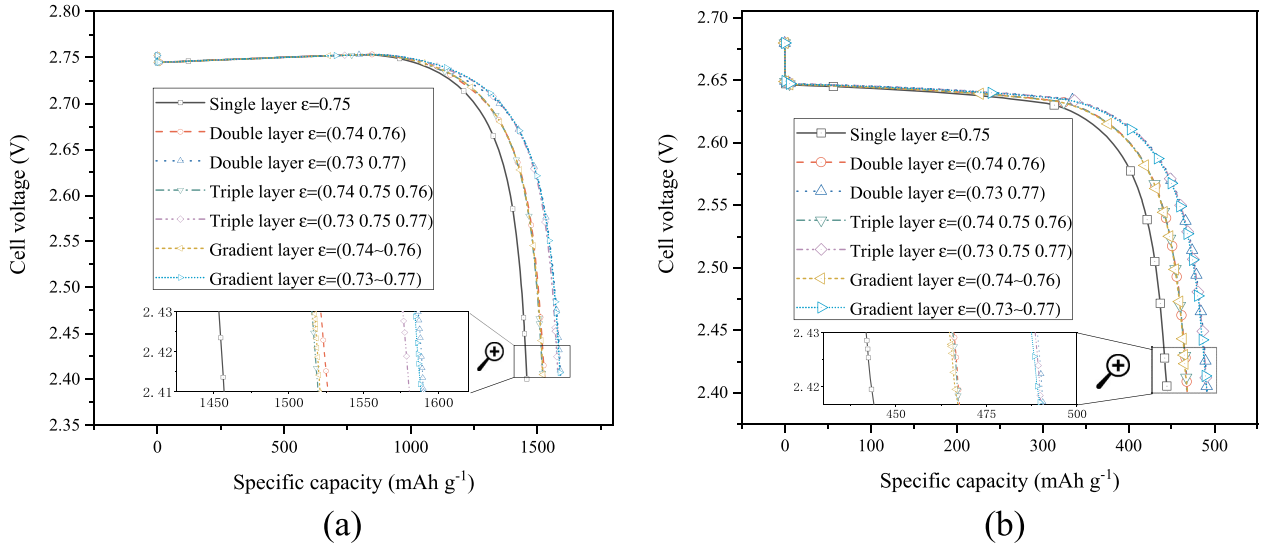


Fig. 7. Voltage-specific capacity curves of different cathode models: (a) discharge current density of 0.05 mA cm^{-2} and (b) discharge current density of 0.2 mA cm^{-2} .

Table 4
Specific capacity (mAh g^{-1}) and improvement.

Cathode type	0.05 mA cm^{-2}		0.2 mA cm^{-2}	
	Specific capacity	Improvement	Specific capacity	Improvement
0.75	1458.4	–	445.1	–
(0.74, 0.76)	1528.8	4.83%	468.1	5.17%
(0.73, 0.77)	1591.5	9.13%	491.3	10.38%
(0.74, 0.75, 0.76)	1520.4	4.25%	467.9	5.12%
(0.73, 0.75, 0.77)	1581.4	8.43%	490.8	10.27%
(0.74–0.76)	1522.6	4.40%	468.5	5.26%
(0.73–0.77)	1589.8	9.01%	491.3	10.38%

where φ_i is the potential in the solution or the solid phase. k_{eff} is effective conductivity of the electrolyte, and σ_{eff} is the effective conductivity of the solid phase.

The effective parameters D_{eff} , k_{eff} , and σ_{eff} are evaluated with Bruggeman relation.

$$D_{Li,eff} = \varepsilon^{1.5} D_{Li}, \quad (11)$$

$$D_{O_2,eff} = \varepsilon^{1.5} D_{O_2}, \quad (12)$$

$$k_{eff} = \varepsilon^{1.5} k, \quad (13)$$

$$\sigma_{eff} = (1 - \varepsilon)^{1.5} \sigma, \quad (14)$$

where D_{Li} and D_{O_2} are the diffusion coefficients of Li^+ and O_2 , respectively. k and σ are the conductivity of the electrolyte and the cathode, respectively.

2.2.4. Electrochemical reaction kinetics

The cathodic reaction rate depends on the concentrations of Li^+ , oxygen, and Li_2O_2 ; therefore, the Butler–Volmer equation is applied in the model [27].

$$\frac{j_c}{nF} = k_a(c_{Li_2O_2,s}) \exp\left[\frac{(1-\beta)nF}{RT}\eta_c\right] - k_c(c_{Li,s})^2(c_{O_2,s}) \exp\left[\frac{-\beta nF}{RT}\eta_c\right], \quad (15)$$

$$\eta_c = \varphi_s - \varphi_l - \Delta\varphi_{film} - E^0, \quad (16)$$

$$\Delta\varphi_{film} = j_c R_{film} \varepsilon_{Li_2O_2}, \quad (17)$$

where k_a and k_c are the two rate coefficients. β is the symmetry factor which is equal to 0.5. η_c is the overpotential at the cathode. $\Delta\varphi_{film}$ is the voltage loss due to the resistance of the discharge product film. E^0 is the theoretical equilibrium potential for the reaction. R_{film} is the resistance of the discharge product film, and $\varepsilon_{Li_2O_2}$ is the volume fraction of solid Li_2O_2 .

The anode electrochemical reaction is described by the general Butler–Volmer equation [27].

$$\frac{j_a}{nF} = i_0 \left\{ \exp\left[\frac{(1-\beta)nF}{RT}\eta_a\right] - \exp\left[\frac{-\beta nF}{RT}\eta_a\right] \right\}, \quad (18)$$

where i_0 is exchange current density. η_a is the overpotential at anode, and the other parameters are identical with the variables described in the earlier equations above.

2.2.5. Insoluble product growth model

As describe earlier the discharge products accumulate on the active surface in the porous cathode. After a certain moment, such products cause pore clogging and active surface decreasing.

The products growth model has been adopted to account for the effect of products on battery performance. In the first model, a max concentration of Li_2O_2 is defined for its low solubility in an electrolyte solution [28]. When the concentration of Li_2O_2 in the solution is lower than the max concentration, then the concentration increases during discharge:

$$\frac{\partial c_{Li_2O_2}}{\partial t} = -\frac{aj_c}{2F}. \quad (19)$$

The concentration of Li_2O_2 in the solution is higher than the max concentration, whereas the porosity and specific area of cathode decrease during discharge:

$$\frac{\partial \varepsilon}{\partial t} = aj_c \frac{M_{Li_2O_2}}{2F \rho_{Li_2O_2}}, \quad (20)$$

$$a = a_0 \left[1 - \left(\frac{\varepsilon_{Li_2O_2}}{\varepsilon_0} \right)^p \right], \quad (21)$$

where $M_{Li_2O_2}$ and $\rho_{Li_2O_2}$ are the relative molecular mass and the density of Li_2O_2 , respectively. a_0 is the initial specific area of the cathode. ε_0 is the initial porosity, and p is a geometrical factor, indicating the

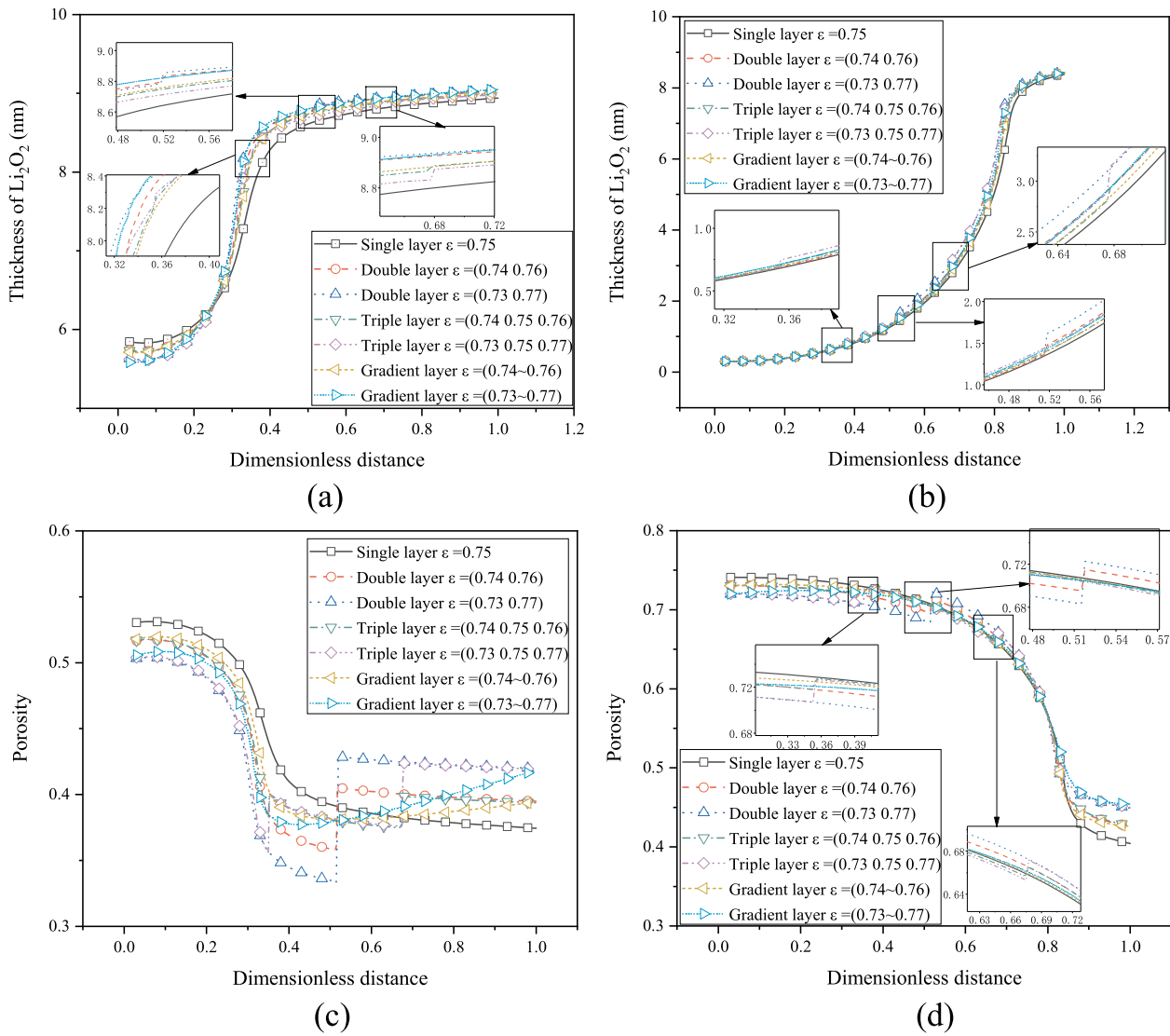


Fig. 8. Product film thickness distribution and cathode porosity distribution at the end of discharge of different cathode models: product film thickness distribution at discharge current density of (a) 0.05 mA cm^{-2} and (b) 0.2 mA cm^{-2} ; cathode porosity distribution at discharge current density of (c) 0.05 mA cm^{-2} and (d) 0.2 mA cm^{-2} .

morphology shape of the solid peroxide. The small values of p mean that the precipitate of Li_2O_2 is plate-like. Conversely, the large values of p indicate a needle-like solid on the active area. In the simulation, these values are set to 0.5 because it is what is usually done.

The tunneling-effect model adopted in this study is related to the electron tunneling effect of the product film. According to studies from Stanford University [51] experimental and theoretical studies have shown a “sudden death” in charge transport when the film thickness ranges from 5 nm to 10 nm. Xue et al. [29] have assumed that electrons may, at most, tunnel through the Li_2O_2 film for 5 nm–10 nm thickness. Therefore, normal distribution is adopted for such assumption, which centers at 7 nm ($l_m = 7 \text{ nm}$) with a width of 2 nm. Thus, the tunneling effect can be described as a probability function.

$$a = a_0 \left[\frac{1 - \text{erf}(l_{\text{Li}_2\text{O}_2} - l_m)}{2} \right], \quad (22)$$

where erf is the error function, and $l_{\text{Li}_2\text{O}_2}$ is the thickness of Li_2O_2 , which can be calculated from

$$l_{\text{Li}_2\text{O}_2} = \left(\frac{\varepsilon_{\text{Li}_2\text{O}_2} + \varepsilon_{s0}}{\varepsilon_{s0}} \right)^{1/3} r_0 - r_0, \quad (23)$$

where ε_{s0} is the initial volume fraction of the solid phase. r_0 is the particle radius in the cathode. $\varepsilon_{\text{Li}_2\text{O}_2}$ is the volume fraction of solid Li_2O_2 , which can be determined from the cathode volume balance:

$$\varepsilon_{\text{Li}_2\text{O}_2} = 1 - \varepsilon - \varepsilon_{s0}, \quad (24)$$

where ε is the volume fraction of liquid electrolyte.

2.3. Boundary and initial conditions

The whole LOB system contains two regions, separator and cathode, and three boundaries. For above governing equations, the boundary and initial conditions are set as follows.

At the interface between air and cathode, a constant oxygen concentration is specified, whereas no-flux conditions are set at other interfaces.

$$c_{\text{O}_2} = c_{\text{O}_2}^0 = c_{\text{O}_2, \text{ext}} \cdot S_{\text{O}_2}, \quad (25)$$

$$\nabla c_{\text{Li}} = 0. \quad (26)$$

And the current density here in the solid phase is equal to the applied

discharge current density while the current density of electrolyte is equal to 0.

$$i_s|_{x=L_c+L_{sep}} = J, \quad i_l|_{x=L_c+L_{sep}} = 0. \quad (27)$$

At the interface between separator and cathode, the current density in the solid phase is equal to 0. And at the interface between Li foil and separator the current density of electrolyte is equal to the applied discharge current density.

$$i_s|_{x=L_{sep}} = 0, \quad i_l|_{x=0} = J. \quad (28)$$

The governing equations and the boundary conditions are discretized using a finite element method and solved by the commercial software package COMSOL Multiphysics on a 32-bit Windows platform with 4 GB RAM and Intel Core i5 3.20 GHz quad-core processor. Table 1 shows the battery dimensions and operating parameters.

2.4. Model validation

The predicted discharge voltage capacity curves of LOB with two different product growth models are compared with the experiment data from Read's work [30], in which Super P (SP-carbon) was used as cathode material, as displayed in Fig. 2.

The model parameters and the applied current density are set according to the experimental apparatus. In general, the predictions achieve acceptable agreement with experimental results. Under different applied current densities, the two product growth models present different performances. The product morphology model prediction fits well with the experimental data under high current density larger than 0.2 mA cm^{-2} . Nevertheless, under the applied current density of 0.05 mA cm^{-2} and 0.1 mA cm^{-2} , the tunneling-effect model achieves an excellent performance. Overall, the simulation results of the tunneling-effect model are superior to the product morphology model. The following work is carried out based on the tunneling-effect model.

3. Parameter sensitivity analysis

If the value of different parameters in the model is changed, then the effect on the specific capacity of the battery at the end of discharge is different. Studying the influence of the parameter variation on the specific capacity of the battery is necessary. In this study, the sensitivity analysis was carried out using the method for proton-exchange membrane fuel cells proposed by Corr ea et al. [41]. Fig. 3 depicts the flow chart of the analysis for non-aqueous LOB.

The formulae for calculating parameter sensitivity are as follows:

$$M_i = \sqrt{\frac{1}{k} \sum_{n=1}^k \left[\frac{G_i(x_n)}{X_n} \right]^2}, \quad (29)$$

$$G_i(x_n) = \frac{g_i(x_0) - g_i(x_n)}{g_i(x_0)}, \quad (30)$$

$$X_n = \frac{x_0 - x_n}{x_0}, \quad (31)$$

where x_0 is the initial value of the parameter (taken from the experimental data). x_n is the different values of the parameters in the parameter analysis ($n = 1, 2, 3, 4$). X_n is the change rate of the value when the parameter is analyzed. $g_i(x)$ is the specific capacity of the battery when the parameter is x . i represents the current density. $G_i(x)$ is the change ratio of the battery-specific capacity when the model calculates the parameter x . k is the number of parameter values ($k = 8$). M_i is the sensitivity of the parameter x when the current density is i .

Table 2 shows the parameters for sensitivity analysis and range of parameter values, where x_0 is the reference value. Then within the range of parameter values, four points different from x_0 which equally spaced

are taken into the above formula for calculation. The reaction rate of anodic current k_a and reaction rate of cathodic current k_c are calculated on a logarithmic basis.

Fig. 4 is the sensitivity curve for 14 important parameters in the LOB model. Many experimental studies have shown that, regardless of the battery composition, the specific capacity is largely determined by the magnitude of the discharge current density [3,4,15,16] and the sensitivity of the same parameter will vary depending on the magnitude of discharge current density. Certain parameter sensitivities increase with the increasing current density, such as the solubility of oxygen and the conductivity of porous cathodes and when the current density is large these parameters show a strong influence on the specific capacity. However, other sensitivities of parameters, such as the anode reaction coefficient, decrease as the current density increases. This correlation may be related to the length of the discharge time. When the current density is small, the battery model discharge process takes longer, which leads to an increase in the influence of such parameters.

In addition, the sensitivities of various parameters differ greatly, such as the porosity sensitivity of the porous cathode is greater than 2.6, and the maximum sensitivity of the separation membrane porosity (0.1 mA cm^{-1}) is less than 0.002. Furthermore, the sensitivities of mostly parameters fluctuate in the same order of magnitude, and their value is relatively stable.

The average sensitivities of the parameters have been obtained from the parameter sensitivities under different current densities. According to the average parameter sensitivity, the parameters are classified into three categories: insensitive, sensitive, and very sensitive, as shown in Table 3. By classification, the extent to which different parameters affect the specific capacity can be seen.

In the LOB model, the specific capacity is substantially affected by several parameters, such as the porosity of the cathode, the thickness of the porous cathode, the solubility factor of oxygen, oxygen diffusion, the particle radius in the cathode, middle product film thickness, and the reaction rate of the cathodic current, as shown in Table 3. The most sensitive parameter is the initial porosity of the cathode with the sensitivity of 3.54, even though a small porosity range was specified and limited within 0.73–0.77. This result matches up with the simulation study of Sahapatsombut [23], where the increase in the specific capacity caused by increasing cathode porosity was found to be greater than that by changing cathode thickness and the cathode reaction coefficient. Furthermore, the parameters related to oxygen transport in the electrolyte solution, such as oxygen solubility factor and oxygen diffusion coefficient, are also sensitive. This indicates that oxygen concentration in the electrolyte has a remarkable influence on the specific capacity of the battery, which agrees with the experimental finds from Read's study [30].

4. Cathode structure optimization

After the model validation, the other parameters related to the discharge products and the cathodes are analyzed along with the voltage specific capacity curve of the battery. These parameters are the discharge product film thickness and the cathode porosity.

In the initial model, the cathode porosity was held constant throughout. Fig. 5 show that the effective porosity and product film's thickness are not uniformly distributed in the cathode. The thickness of the product film near the air is relatively large, and the thickness of the product film near the side of the lithium anode is small. Thus, the effective porosity decreases as one goes toward the air. Moreover, as the discharge progresses, the differences between film thickness and porosity of the product on both sides of the cathode widen. The discharge product accumulates on the air inlet side, making the diffusion of oxygen in the cathode difficult, and the active surface inside the cathode cannot react with oxygen.

In addition, the initial porosity of the cathode is the most sensitive parameter among all sensitivity analysis parameters which means the

initial porosity is a significant factor affecting the specific capacity. Hence, adjusting the initial porosity of the porous cathode will inevitably have a greater impact on the specific capacity of the battery.

Though the above calculations and analysis, a cathode with layered porosity is proposed. Specifically, the cathodes are divided into several layers, and the cathode porosity of each layer is different. In this study, the porosity of the cathode near the air side is set to a large value to improve material transport performance and store discharge products. The porosity of the cathode layer near the negative side of the metal lithium is set to a small value to ensure cathode conductivity, active-specific surface area, and structural strength. For quantitative analysis, the average porosity of the cathode has been kept constant during the study. The effects of two-layer, three-layer, and gradient porosity cathodes on battery-specific capacity and cathode structure evolution during discharge are studied. Fig. 6 shows the hierarchical cathodes. Ren [31] measured the porosity of the SP-carbon cathode porosity by a thickness method, which value is 0.753 ± 0.022 . So the range of the layered cathode's porosity is determined from 0.73 to 0.77, and the porosity range from 0.74 to 0.76 is also set for comparison.

The three different cathode structure models above are brought into the multiphysics-coupled LOB model and are then calculated. The initial porosity distribution of each cathode structure is divided into two types. The two-layer cathode porosity has two distributions of 0.73, 0.77, and 0.74, 0.76, abbreviated as (0.73 0.77) and (0.74 0.76). The three-layer cathode is (0.73 0.75 0.77) and (0.74 0.75 0.76). The gradient porosity cathodes are (0.73–0.77) and (0.74–0.76).

Through calculation, the cathode with adjusted pore distribution improves the specific capacity of the battery, as shown in Fig. 7. The voltage-specific capacity curves almost completely coincide when the two-layer cathode, three-layer cathode and gradient porosity cathode have the initial porosity distributions of (0.74 0.76), (0.74 0.75 0.76) and (0.74–0.76) respectively. And the situation is similar with the two-layer, three-layer, and gradient porosity cathodes with (0.73 0.77), (0.73 0.75 0.77) and (0.73–0.77) porosities, which specific capacities are higher than the previous cases.

Table 4 shows that the hierarchical cathodes with the same cathode porosity span are similar to the increase in the specific capacity of the battery. The cathode with a porosity span of 0.73–0.77 has the largest specific capacity increase of the battery, and the maximum increase is 10.38%.

The model also calculates the product film thickness distribution and porosity distribution in the porous cathode. The hierarchical structure of the cathode changes the product and porosity distributions in the cathode during discharge, as shown in Fig. 8. The film thickness and the porosity of the product show a segmented distribution at the end of the discharge. The characteristics of the segmentation distribution when the discharge current density is 0.05 mA cm^{-2} are evident.

Nomenclature

a	specific interfacial area ($\text{m}^2 \text{ m}^{-3}$)
c_i	concentration of species i (mol m^{-3})
$c_{i,s}$	concentration of species i at the electrode active surface (mol m^{-3})
$c_{\text{max,Li}_2\text{O}_2}$	solubility limit of Li_2O_2 dissolved in electrolyte (mol m^{-3})
Da	Damköhler number
D_i	diffusion coefficient of species i ($\text{m}^2 \text{ s}^{-1}$)
$D_{i,\text{eff}}$	effective diffusion coefficient of species i ($\text{m}^2 \text{ s}^{-1}$)
E	cathode potential (V)
E^0	cathode potential at standard state (V)
f	activity coefficient of LiPF_6 salt
F	Faraday's constant ($96485.34 \text{ C mol}^{-1}$)
i_l	current density in the liquid phase (A m^{-2})
i_s	current density in the solid phase (A m^{-2})
J	applied current density (A m^{-2})

The calculation has also found that the average product film thickness in the hierarchical cathode increases, and the average porosity decreases at the end of the discharge compared with the single layer cathode. This finding shows that numerous discharge products are stored in the cathode, thereby increasing the specific capacity of the battery.

5. Conclusion

This study presented a comprehensive one-dimensional model on LOB's performance and compared the calculation results of two different insoluble discharge product growth models. The first product growth model, called the product morphology model, calculates the specific surface area according to the morphology of the solid peroxide Li_2O_2 . The other model, called the tunneling-effect model, adopts a probability function to take into account the influence of electron tunneling effect on the specific surface area. The two models show acceptable agreement with the experimental data from literature with the tunneling effect model showing the best fit and was selected for the rest of the paper.

The parameter sensitivity analysis of the model also demonstrates that the initial porosity of the porous cathode has the greatest influence on the specific capacity of the discharge process. In addition, from the calculation results of the LOB model with the tunneling-effect sub-model, the product and porosity distributions in the cathode are not uniform at the end of the discharge. Thus, we have proposed hierarchical porous cathodes comprising two-layer, three-layer, and gradient porosity cathodes. The hierarchical cathode helps to improve the distribution of discharge products in the cathode and increased the specific capacity by up to 10.38% with the two-layer and gradient porosity designs. The future work can refer to the results of the parameter sensitivity analysis in this paper to design LOBs with better performances both in experiment and simulation.

Declaration of competing interest

The authors declare that they have no known competing financial interests or personal relationships that could have appeared to influence the work reported in this paper.

Acknowledgments

This work was supported by the National Natural Science Foundation of China (No. 51676013). L. Liu would like to acknowledge the support from the National Science Foundation under Grant Number 1840732. In the meanwhile, L. Liu would like to thank the support from KS NASA EPSCoR program, KU Research GO awards, and KU General Research Fund.

j	interfacial transfer current density (A m^{-2})
k	reaction rate constant
$l_{\text{Li}_2\text{O}_2}$	thickness of the Li_2O_2 film (m)
l_m	middle thickness of the Li_2O_2 film (m)
L_c, L_{sep}	thickness of the porous cathode and separator
m_i	mass of species i (kg)
$M_{\text{Li}_2\text{O}_2}$	symbol for the chemical formula or molecular weight of Li_2O_2
M_i	sensitivity of the parameter x when the current density is i
n	number of electrons transferred in the electrode reaction
N_i	molar flux of species i ($\text{mol m}^{-3} \text{s}^{-1}$)
p	surface effect factor
r	particle radius (m)
R	universal gas constant ($8.3143 \text{ J mol}^{-1} \text{ K}^{-1}$)
R_i	reaction rate term that accounts for electrochemical and chemical reactions ($\text{mol m}^{-3} \text{ s}^{-1}$)
R_{film}	electrical resistivity across Li_2O_2 film ($\Omega \text{ m}^2$)
s_i	stoichiometric coefficient of species i in electrode reaction
S_{O_2}	solubility factor of O_2 in non-aqueous electrolyte
t	time (s)
t_+	transference number of cation in electrolyte
T	temperature (K)
X_n	the change rate of the parameter value
z_i	valence of charge number of species i

Greek letters

β	Symmetry factor
ε	Porosity
η	surface or activated overpotential (V)
κ	conductivity of electrolyte (S m^{-1})
κ_{eff}	effective conductivity of electrolyte (S m^{-1})
ν	number of moles of ions into which a mole electrolyte dissociate
ν_+	numbers of moles cations produced by the dissociation of a mole of electrolyte
ρ_i	density of species i (kg m^{-3})
σ	conductivity of electrode (S m^{-1})
σ_{eff}	effective conductivity of electrode (S m^{-1})
φ	electric potential (V)
$\Delta\varphi_{\text{film}}$	voltage drop across Li_2O_2 film (V)
∇	differential operator

Subscripts and Superscripts

0	initial
a	anode
c	cathode
l	liquid phase
s	solid phase

References

- [1] A.C. Luntz, B.D. McCloskey, Nonaqueous Li-air batteries: a status report, *Chem. Rev.* 114 (2014) 11721–11750.
- [2] J.P. Zheng, R.Y. Liang, M. Hendrickson, E.J. Plichta, Theoretical energy density of Li-air batteries, *J. Electrochem. Soc.* 155 (2008) A432.
- [3] T. Ogasawara, A. Débart, M. Holzapfel, P. Novák, P.G. Bruce, Rechargeable Li_2O_2 electrode for lithium batteries, *J. Am. Chem. Soc.* 128 (2006) 1390–1393.
- [4] Y. Lu, D.G. Kwabi, K.P.C. Yao, J.R. Harding, J. Zhou, L. Zui, Y. Shao-Horn, The discharge rate capability of rechargeable Li-O₂ batteries, *Energy Environ. Sci.* 4 (2011) 2999.
- [5] W. Xu, K. Xu, V.V. Viswanathan, S.A. Towne, J.S. Hardy, J. Xiao, Z. Nie, D. Hu, D. Wang, J. Zhang, Reaction mechanisms for the limited reversibility of Li-O₂ chemistry in organic carbonate electrolytes, *J. Power Sources* 196 (2011) 9631–9639.
- [6] M. Augustin, P.E. Vullum, F. Vullum-Bruer, A.M. Svensson, Inside the electrode: looking at cycling products in Li/O₂ batteries, *J. Power Sources* 414 (2019) 130–140.
- [7] W. Xu, J. Wang, F. Ding, X. Chen, E. Nasybulin, Y. Zhang, J. Zhang, Lithium metal anodes for rechargeable batteries, *Energy Environ. Sci.: EES (Ecotoxicol. Environ. Saf.)* 7 (2014) 513–537.
- [8] K. Sakai, S. Iwamura, S.R. Mukai, Influence of the porous structure of the cathode on the discharge capacity of lithium-air batteries, *J. Electrochem. Soc.* 164 (2017) A3075–A3080.
- [9] Z. Ma, X. Yuan, L. Li, Z. Ma, D.P. Wilkinson, L. Zhang, J. Zhang, A review of cathode materials and structures for rechargeable lithium-air batteries, *Energy Environ. Sci.* 8 (2015) 2144–2198.
- [10] C. Xia, M. Waletzko, L. Chen, K. Pepler, P.J. Klar, J. Janek, Evolution of Li_2O_2 growth and its effect on kinetics of Li-O₂ batteries, *ACS Appl. Mater. Interfaces* 6 (2014) 12083–12092.
- [11] X. Li, J. Huang, A. Faghri, A critical review of macroscopic modeling studies on Li-O₂ and Li-air batteries using organic electrolyte: challenges and opportunities, *J. Power Sources* 332 (2016) 420–446.
- [12] D. Sharon, D. Hirshberg, M. Afri, A. Garsuch, A.A. Frimer, D. Aurbach, Lithium•Oxygen electrochemistry in non-aqueous solutions, *Isr. J. Chem.* 55 (2015) 508–520.
- [13] Z. Peng, S.A. Freunberger, L.J. Hardwick, Y. Chen, V. Giordani, F. Bardé, P. Novák, D. Graham, J. Tarascon, P.G. Bruce, Oxygen reactions in a non-aqueous Li+ electrolyte, *Angew. Chem. Int. Ed.* 50 (2011) 6351–6355.
- [14] J. Shui, J.S. Okasinski, C. Chen, J.D. Almer, D. Liu, In operando spatiotemporal study of Li_2O grain growth and its distribution inside operating Li-O(2) batteries, *ChemSusChem* 7 (2014) 543.
- [15] B.D. Adams, C. Radtke, R. Black, M.L. Trudeau, K. Zaghbi, L.F. Nazar, Current density dependence of peroxide formation in the Li-O₂ battery and its effect on charge, *Energy Environ. Sci.* 6 (2013) 1772.
- [16] S. Lau, L.A. Archer, Nucleation and growth of lithium peroxide in the Li-O₂ battery, *Nano Lett.* 15 (2015) 5995–6002.
- [17] Y. Wang, Modeling discharge deposit formation and its effect on lithium-air battery performance, *Electrochim. Acta* 75 (2012) 239–246.

- [18] U. Sahapatsumbut, H. Cheng, K. Scott, Modelling of electrolyte degradation and cycling behaviour in a lithium–air battery, *J. Power Sources* 243 (2013) 409–418.
- [19] C.Y. Jung, T.S. Zhao, L. An, Modeling of lithium–oxygen batteries with the discharge product treated as a discontinuous deposit layer, *J. Power Sources* 273 (2015) 440–447.
- [20] X. Li, J. Huang, A. Faghri, Modeling study of a Li–O₂ battery with an active cathode, *Energy* 81 (2015) 489–500.
- [21] J. Huang, A. Faghri, Analysis of electrolyte level change in a lithium air battery, *J. Power Sources* 307 (2016) 45–55.
- [22] X. Li, A modeling study of the pore size evolution in lithium–oxygen battery electrodes, *J. Electrochem. Soc.* 162 (2015) A1636–A1645.
- [23] K. Scott, H. Cheng, U. Sahapatsumbut, Modelling the micro–macro homogeneous cycling behaviour of a lithium–air battery, *J. Power Sources* 227 (2013) 243–253.
- [24] V. Esfahanian, M.T. Dalakeh, N. Aghamirzaie, Mathematical modeling of oxygen crossover in a lithium–oxygen battery, *Appl. Energy* 250 (2019) 1356–1365.
- [25] C. Gaya, Y. Yin, A. Torayev, Y. Mammeri, A.A. Franco, Investigation of bi-porous electrodes for lithium oxygen batteries, *Electrochim. Acta* 279 (2018) 118–127.
- [27] N.P. Balsara, J.S. Newman, *Electrochemical Systems*, fourth ed., 2019.
- [28] K. Tasaki, A. Goldberg, J. Lian, M. Walker, A. Timmons, S.J. Harris, Solubility of lithium salts formed on the lithium–ion battery negative electrode surface in organic solvents, *J. Electrochem. Soc.* 156 (2009) A1019.
- [29] K. Xue, T. Nguyen, A.A. Franco, Impact of the cathode microstructure on the discharge performance of lithium air batteries: a multiscale model, *J. Electrochem. Soc.* 161 (2014) E3028–E3035.
- [30] J. Read, Characterization of the lithium/oxygen organic electrolyte battery, *J. Electrochem. Soc.* 149 (2002) A1190.
- [31] X. Ren, S.S. Zhang, D.T. Tran, J. Read, Oxygen reduction reaction catalyst on lithium/air battery discharge performance, *J. Mater. Chem.* 21 (2011) 10118.
- [32] J. Zhang, D. Wang, W. Xu, J. Xiao, R.E. Williford, Ambient operation of Li/Air batteries, *J. Power Sources* 195 (2010) 4332–4337.
- [33] S.G. Stewart, J. Newman, The use of UV/vis absorption to measure diffusion coefficients in LiPF₆ electrolytic solutions, *J. Electrochem. Soc.* 155 (2008) F13.
- [34] Y. Lu, D.G. Kwabi, K.P.C. Yao, J.R. Harding, J. Zhou, L. Zuin, Y. Shao-Horn, The discharge rate capability of rechargeable Li–O₂ batteries, *Energy Environ. Sci.* 4 (2011) 2999.
- [35] W. Xu, J. Xiao, J. Zhang, D. Wang, J. Zhang, Optimization of nonaqueous electrolytes for primary lithium/air batteries operated in ambient environment, *J. Electrochem. Soc.* 156 (2009) A773.
- [36] P. Andrei, J.P. Zheng, M. Hendrickson, E.J. Plichta, Some possible approaches for improving the energy density of Li–air batteries, *J. Electrochem. Soc.* 157 (2010) A1287.
- [37] A. Nyman, M. Behm, G. Lindbergh, E. Kemiteknik, K.T.H. Tillämpad, F.K.C. Skolan, Electrochemical characterisation and modelling of the mass transport phenomena in LiPF₆–EC–EMC electrolyte, *Electrochim. Acta* 53 (2008) 6356–6365.
- [38] Q. Li, H.Y. Sun, Y. Takeda, N. Imanishi, J. Yang, O. Yamamoto, Interface properties between a lithium metal electrode and a poly(ethylene oxide) based composite polymer electrolyte, *J. Power Sources* 94 (2001) 201–205.
- [39] S.L.W. Weaver, B.J. McCall, *CRC Handbook of Chemistry and Physics*, 87th ed, American Chemical Society, 2007, p. 724.
- [40] H. Cheng, K. Scott, Selection of oxygen reduction catalysts for rechargeable lithium–air batteries—metal or oxide? *Appl. Catal. B Environ.* 108 (2011) 140–151.
- [41] J.M. Correa, F.A. Farret, V.A. Popov, M.G. Simoes, Sensitivity analysis of the modeling parameters used in simulation of proton exchange membrane fuel cells, *IEEE Trans. Energy Convers.* 20 (2005) 211–218.
- [42] L. Ma, T. Yu, E. Tzoganakis, et al., Fundamental understanding and material challenges in rechargeable nonaqueous Li–O₂ batteries: recent progress and perspective, *Adv. Energy Mater.* 8 (22) (2018) 1800348.
- [43] J. Fu, X. Guo, H. Huo, Y. Chen, T. Zhang, Easily decomposed discharge products induced by cathode construction for highly energy-efficient lithium–oxygen batteries, *ACS Appl. Mater. Interfaces* 11 (2019) 14803–14809.
- [44] T.K. Zakharchenko, M.V. Avdeev, A.V. Sergeev, A.V. Chertovich, O.I. Ivankov, V. I. Petrenko, Y. Shao-Horn, L.V. Yashina, D.M. Itkis, Small-angle neutron scattering studies of pore filling in carbon electrodes: mechanisms limiting lithium–air battery capacity, *Nanoscale* 11 (2019) 6838–6845.
- [45] M. Augustin, P.E. Vullum, F. Vullum-Bruer, A.M. Svensson, Inside the electrode: looking at cycling products in Li/O₂ batteries, *J. Power Sources* 414 (2019) 130–140.
- [46] M. Jeong, W. Kwak, M. Islam, J. Park, H.R. Byon, M. Jang, Y. Sun, H. Jung, Triple hierarchical porous carbon spheres as effective cathodes for Li–O₂ batteries, *J. Electrochem. Soc.* 166 (2019) A455–A463.
- [47] K. Sakai, S. Iwamura, S.R. Mukai, Influence of the porous structure of the cathode on the discharge capacity of lithium–air batteries, *J. Electrochem. Soc.* 164 (2017) A3075–A3080.
- [48] P. Tan, W. Shyy, L. An, Z.H. Wei, T.S. Zhao, A gradient porous cathode for non-aqueous lithium–air batteries leading to a high capacity, *Electrochem. Commun.* 46 (2014) 111–114.
- [49] W. Mu, X. Liu, Z. Wen, et al., Numerical simulation of the factors affecting the growth of lithium dendrites, *J. Energy Storage* 26 (2019) 100921.
- [50] N. Meng, F. Lian, Y. Li, X. Zhao, L. Zhang, S. Lu, H. Li, Exploring PVFM-based janus membrane-supporting gel polymer electrolyte for highly durable Li–O₂ batteries, *ACS Appl. Mater. Interfaces* 10 (2018) 22237–22247.
- [51] V. Viswanathan, K.S. Thygesen, J.S. Hummelshøj, J.K. Nørskov, G. Girishkumar, B. D. McCloskey, A.C. Luntz, Electrical conductivity in Li₂O₂ and its role in determining capacity limitations in non-aqueous Li–O₂ batteries, *J. Chem. Phys.* 135 (2011) 214704.